KADI

Support for an African Earth System Model

Deliverable 2.1. HORIZON-INFRA-2021-DEV-01-02

Funded by
the European Union

kadi-project.eu

KADI

PROJECT NUMBER	OFFICIAL NAME	EXTERNAL COMMUNICATIONS NAME
HORIZON-INFRA-2021-DEV-01-02	KADI Knowledge and climate services from an African observation and Data research Infrastructure	KADI
DUE DATE OF DELIVERABLE	**REFERENCE WP AND TASK**	**BENEFICIARY IN CHARGE**
03.02.2025 Status submitted Update due 31.08.2025	WP2 AND TASK 2.1	WITS
PROJECT URL		**EU PROJECT OFFICER**
https://www.kadi-project.eu		Pierre Quertenmont

VERSION LOG

NAME	DATE	AUTHORS	COMMENTS

LIST OF AUTHORS

NAME	INSTITUTION
Francois Engelbrecht	WITS
Jessica Steinkopf	WITS
Yolandi Ernst	WITS
Caroline Hardy	WITS
Gregor Feig	SAEON
Nolusindiso Ndara	SAEON
Amukelani Maluleke	SAEON

KADI

Executive Summary

Earth System models (ESMs) are global climate models that can explicitly represent biogeochemical processes, first and foremost, those related to the carbon cycle. In this pilot, we focused on evaluating and making specific improvements to the parametrizations of land-surface attributes in an Earth System Model that is central to providing a range of climate services in Africa. The model consists of the conformal-cubic atmospheric model (CCAM) developed by the Commonwealth Scientific and Industrial Research Organisation (CSIRO) in Australia and a dynamic land-surface model, CABLE (CSIRO Atmosphere Biosphere Land Exchange). This modelling system has flexible downscaling capabilities, adopting a spectral nudging methodology, and can be integrated as a quasi-uniform global model or a stretched-grid, variable-resolution regional model to obtain high resolution over a domain of interest. Simulations were conducted in which the model was nudged using ERA5 reanalysis data, thereby ensuring the simulations were consistent with historical weather patterns as captured in the reanalysis outputs. This enabled the evaluation of several land-atmosphere fluxes and attributes of the simulated model outputs against flux tower observations, as well as Earth observation data products. Data to verify the model's representation of significant exchanges between the land surface and atmosphere, including the carbon, energy and water fluxes, was obtained from six different EFTEON flux tower sites in South Africa, representing a range of biomes and environmental settings, for the period 2020 – 2023. For the earth observation component, satellite-derived soil moisture data were validated against three flux tower-measured soil moisture values and then compared to the model's soil moisture outputs. Additionally, a spatial correlation was conducted between remotely sensed biomass and modelled carbon flux estimations. Overall, the modelling system does exceptionally well at capturing the key attributes of the seasonal and diurnal cycles of certain land-atmosphere fluxes. A good agreement between satellite-derived soil moisture and the modelled soil moisture further supports the model's capability to represent land-atmosphere fluxes. Annual total biomass and biomass changes did not show strong spatial correlations with carbon flux estimations, most likely due to limitations imposed by the biomass data and biomass only representing one component of the carbon flux process. The skill of the model does vary by site, however, highlighting the importance of validating the model across different biomes and climatic zones. Validation with Earth observation data holds considerable promise for identifying hotspots of carbon flux interannual variations and their underlying drivers across Africa but will require additional in situ observations. In this KADI pilot study, it was therefore clear that an extended observation network would also be valuable for validating satellite data. Such verification work is critical to enable confident use of earth observation and ESMs combined with in situ observations, to identify hotspots of land-atmosphere fluxes. Additionally, identifying such biases is crucial for future model development and enhancing the parameterizations of land-atmosphere attributes in ESMs, particularly over Africa. The better ESMs represent these complex processes, the more reliable their projections of future climate change are, which is critical for informing mitigation and adaptation strategies on the continent. This research provides the basis for further validation to continuously improve the ESM.

KADI

CONTENTS

KADI

Introduction

Global Climate Models (GCMs) are the primary tools used to study and project climate changes. GCMs simulate the physical aspects of the climate system (atmosphere, ocean, land surface, and sea ice). These models are based on the fundamental laws of physics, solving equations to model climate variables such as precipitation, temperature and circulation patterns, among others (GFDL, 2025). While GCMs focus on climate dynamics, Earth System Models (ESMs) build on GCMs, adding biological and chemical processes for a more comprehensive simulation of Earth's climate system. ESMs include additional components that represent biogeochemical cycles, for example, the carbon cycle and vegetation dynamics (Bonan and Doney, 2018; Kawamiya et al., 2020). This means that ESMs can simulate interactions between the climate system and ecosystems, making them useful tools for studying feedback mechanisms, such as how carbon dioxide (CO_2) emissions affect the climate, and how climate change impacts ecosystems. These models are vital tools for developing informed climate change adaptation and mitigation strategies.

As global interest in climate change grew and the importance of carbon cycle feedbacks in accelerating climate change became evident (Cox et al., 2000; Friedlingstein et al., 2001), several institutes enhanced traditional GCMs by incorporating new components, leading to the development of Earth System Models (ESMs). Therefore, several ESMs exist and are widely used, each developed by leading research institutions. To mention a few, there is the Community Earth System Model (CESM) developed by the United States National Centre for Atmospheric Research (NCAR, 2025); the ICOsahedral Nonhydrostatic (ICON) Model developed by the Max Planck Institute for Meteorology and the German Weather Service (nextGEMS, 2025); the Unified Model (UM) developed by the United Kingdom Met Office (Met Office, 2025); and the Model for Interdisciplinary Research on Climate (MIROC)-based ESM developed jointly by the Japan Agency for Marine-Earth Science and Technology, Centre for Climate System Research of the University of Tokyo, and the National Institute for Environmental Studies (Kawamiya et al., 2020). These, and other ESMs, have many applications and have been widely used to study the complex interactions of the earth system.

Bonan and Doney (2018) state that reducing the sources and enhancing the sinks of long-lived greenhouse gases are the most direct means to mitigate anthropogenic climate change. Thus, it is important to study terrestrial and ocean fluxes to understand when and where they act as sinks and sources, and ESMs enable such investigations. Furthermore, ESMs are used to study other environmental concerns such as ocean acidification through ocean uptake of emitted carbon and the implications of land use change related to biofuel production, agriculture expansion, and urbanization. It is also valuable in carbon accounting, contributing to the top-down estimation of carbon budget components, when bottom-up methods are inadequate (e.g. Friedlingstein et al. 2024). The latter is especially applicable to Africa (e.g. Ernst et al. 2024). Hazeleger et al. (2010) suggest that ESMs bridge the gap between numerical weather predictions and climate models, thereby having a wide range of applications, from earth system research to providing practical climate information for a diverse range of users. Therefore, the accuracy of ESMs in projecting climate change and climate variables is crucial for advancing Earth system research and supporting informed climate decision-making.

However, ESMs are the most complex in the hierarchy of models simulating the earth's interacting atmosphere-land-ocean-sea ice system, integrating biogeochemical processes to improve climate simulations (Bonan and Doney, 2018). This added complexity also introduces greater uncertainty in

predictions (Collins et al., 2011), highlighting the need for systematic validation and evaluation. Several studies emphasize the importance of verifying ESMs to improve their reliability. Regular model evaluation helps benchmark improvements across model generations, assess consistency with observations, and refine parameterizations (Lee et al., 2024). Such verification enhances confidence in model outputs, ultimately reducing uncertainty in climate change projections and improving their usefulness for policymakers and stakeholders (Flato et al., 2014; Eyring et al., 2019). However, traditional model evaluation methods struggle to keep pace with the increasing model complexity, and it is therefore critical that more advanced validation tools and approaches are developed, ensuring models are compared against observations for multiple variables and timescales (Eyring et al., 2019). Given the complexity of ESMs, validation should be done on the different components of the model.

Observing land-atmosphere interactions remains essential for understanding the effects of climate change on the sources and sinks of greenhouse gases, and the eddy covariance (EC) technique has proven to be a viable method for long-term measurement of fluxes at ecosystem scales. The EC technique measures heat, mass, and momentum exchanges between a flat, horizontally homogeneous surface and the overlying atmosphere. The net transport between the surface and atmosphere is one-dimensional, and the vertical flux density can then be calculated by the covariance between the turbulent fluctuations of the vertical wind (movement up and down) and the content of the gas of interest (CO_2 or H_2O) in these upward and downward moving air parcels (Baldocchi, 2003). The contributing area to these measurements is known as the footprint and varies as its dimensions and orientation are dependent on measuring height, surface roughness and atmospheric stability, surface roughness length, wind speed and direction (Schmid and Lloyd, 1999).

While the EC technique is a robust direct measurement technique providing ground-based data, it does not capture substantial spatial scale variability in climate and ecosystem-related parameters. In addition, setting up EC flux towers is expensive. Thus, they have been sparse on the African continent due to limited funding and the lack of environmental and climate research priorities in some African regions. Despite these challenges, several studies in southern Africa have used the in situ measurement of ecosystem variables such as carbon dioxide flux (Net Ecosystem Exchange) applying the eddy covariance technique (e.g. Archibald et al., 2009; Kutsch et al., 2008; Räsänen et al., 2017; Rybchak et al., 2020).

Measurements of net ecosystem exchange, latent heat and sensible heat using the EC technique help towards understanding the behaviour, vulnerability and resilience of ecosystems in relation to climate change and anthropogenic impacts such as land-use change and agricultural expansion. For example, terrestrial ecosystems provide a crucial service in reducing the accumulation of anthropogenic CO_2 in the atmosphere, thus, understanding the net CO_2 flux is vital in identifying terrestrial CO_2 sources and sinks. Furthermore, latent heat and sensible heat are parameters that are crucial for Earth's surface energy budget. For ESMs, it is important to accurately represent the exchanges of energy between the surface and the atmosphere in order to model the Earth's climate and project changes in temperature, heat distribution and overall climate behaviour. From an ecosystem perspective, H and LE also help understand evapotranspiration. In addition, combining H and LE provides significant information on how available energy affects the distribution of water vapour and precipitation patterns - an important component for ESMs to simulate the water cycle and improve the understanding of regional and global hydrological dynamics.

To resolve the spatial limitations of eddy covariance flux tower availability, earth observation data can be employed to quantify terrestrial carbon stock changes and its associated drivers to assess regional biases in earth system models. For instance, dryland (savanna and grassland) ecosystems are known to have a dominant contribution to the global interannual variability of land-atmosphere CO_2 fluxes (Ahlström et al., 2015), but these systems are usually poorly described in state-of-the art Earth System Models in terms of vegetation types, fire-vegetation interactions and access to soil moisture by deep rooted shrubs and trees. By leveraging more recent EO datasets and in situ observation network to estimate aboveground biomass changes and soil moisture, we can evaluate carbon stock dynamics and its relationships to various processes.

Measurements of soil moisture present a key component in the carbon cycle (Hao et al. 2025) as it governs soil organic matter (SOM) formation and decomposition photosynthesis, and microbial activity (e.g. Heckman et al. 2023). Optimal moisture levels promote carbon sequestration by stabilizing organic matter on mineral surfaces and supporting diverse microbial communities, while drought or excessive flooding can disrupt these processes, impacting the global carbon balance (Hao et al. 2025). Soil moisture also creates indirect links to the atmosphere, affecting water and carbon exchanges between land and air, influencing the global carbon sink. Satellite missions retrieve near-surface soil moisture (top ~0–5 cm) by measuring microwave signals that respond to the water content of the soil, typically reported in m^3/m^3 (or %). Passive L-band radiometers like SMAP and SMOS sense natural microwave emission and, using radiative-transfer (τ–ω) models, estimate soil moisture at ~9–36 km resolution every 2–3 days; active C-band scatterometers (e.g., ASCAT) infer moisture from backscatter changes at ~12–25 km with daily coverage (Jackson et al. 2012; Entekhabi et al. 2010; Chen et al. 2018). These products are most reliable over bare to moderately vegetated surfaces and can be limited by dense canopies, surface roughness, standing water, and radio-frequency interference. These products are widely used for drought monitoring, crop and rangeland assessment, fire risk, hydrologic forecasting, and to evaluate or bias-correct model outputs using in situ probes or flux tower soil moisture (Reichle et al. 2017).

Using satellite-derived above-ground biomass (AGB) to verify ESMs is powerful because it constrains the state of the carbon pool that integrates years of net fluxes, allowing checks on spatial patterns (gradients with climate, soils, land use) and on multi-year trends (dAGB) against modelled stocks and stock changes. There are, however, key caveats, including the scale and timing mismatches, inconsistencies in data retrieval methodology, disturbance bookkeeping (e.g., harvest, fire, and mortality shift biomass without immediately appearing in some products or models), and the need for intensive verification with field data. Nevertheless, despite biomass not being directly comparable to NEE, it can be used to track trends over large spatial extents.

Therefore, the main objective of this study is to use in situ data to validate the ESM CCAM-CABLE (*see Data and Methods*) representation of significant processes, namely, net ecosystem exchange, latent heat and sensible heat fluxes at six EFTEON eddy covariance flux tower sites in South Africa representing a range of biomes and environmental characteristics at the diurnal, seasonal and annual scales. Additionally, the study aims to validate Earth observation estimates of above-ground biomass and soil moisture against observations from the same set of flux towers, providing a baseline comparison of satellite data against the ESM that can be refined in future.

KADI

Data and Methods

Study area and flux tower instruments

This study utilized flux tower data from six different sites across South Africa, which were operated and maintained by the Expanded Freshwater and Terrestrial Environmental Observation Network (EFTEON), a component of the South African Environmental Observation Network (SAEON). These sites are Benfontein Karoo, Benfontein Savanna, Cathedral Peak, Jonkershoek, Maputaland and Spioenkop, and have unique characteristics and instruments (Table 1).

Table 1: Study sites from which observations were obtained

Stations	**Benfontein Karoo**	**Benfontein Savanna**	**Cathedral Peak**	**Jonkershoek**	**Maputaland**	**Spioenkop**
Biome	Nama-Karoo	Savanna	Grassland	Fynbos	Indian ocean coastal belt, savanna and forest	Grassland
Climate	Semi-arid with mean annual rainfall of 419 ±132 (70 - 500) mm/yr with most of it falling in the warmer months (Oct to April). Temperatures range from 5○C to 43○C.	Semi-arid with mean annual rainfall of 419 ±132 (200 – 1350) mm/yr with most of it falling in the warmer months (Oct to April). Maximum temperature is always above 26○C and can exceed 32○C.	Falls within summer rainfall region with wet, humid summers and cold dry winters. The catchment typically receives ~109 mm of precipitation and has 163.38 rainy days annually. The area's yearly temperature is 23○C.	Characterized by Mediterranean climate with wet cold winters and hot dry summers. The mean annual precipitation ranges from 1104-1539 mm/yr. Temperatures in summer range between 25○C and 35○C, while the winter averages around 10○C.	Situated between the tropical and subtropical zones, characterized by hot summers and mild winters with mean annual temperature of 22○C, Mean daily temperatures vary from 21.0 °C to 32.1 °C in summer and 10.9 °C to 26.4 °C in winter. The region has dry winter months with a mean annual summer rainfall between 500 mm to 750 mm.	Experiences a warm-temperate climate, with rainfall averages of 814 mm/yr falling mainly in summer. Temperatures range between
Location	28°51'38.9" S, 24°50'39.1" E	28°53'43.6" S, 24°51'66.7" E	28°56'40.8" S, 29°15'48.1" E	33°59'17.7" S, 18°57'50.2" E	27°23'42.8" S, 32°35'20.4" E	28°42'13.5" S, 29°31'30.9" E
Flux Tower Instrumentation						
Gas Analyser	IRGASON (Campbell Sci) mounted at 3.5m	IRGASON (Campbell Sci) mounted at 10.5m	IRGASON (Campbell Sci) mounted at 6m	IRGASON (Campbell Sci) mounted at 6m	IRGASON (Campbell Sci) mounted at 6m	IRGASON (Campbell Sci) mounted at 6m

Air Temperature and Humidity Probe	Campbell Sci HygroVUE^{TM}10 mounted at 2m	Campbell Sci HygroVUE^{TM}10 mounted at 2m	Campbell Sci HygroVUE^{TM}10 mounted at 2m	Campbell Sci HygroVUE^{TM}10 mounted at 2m	Campbell Sci HygroVUE^{TM}10 mounted at 2m	Campbell Sci HygroVUE^{TM}10 mounted at 2m
Wind Speed and Direction	RM Young Anemometer and Vane (03002)	RM Young Anemometer and Vane (03002)				
Data Availability	15/01/2020 - 30/04/2023	30/01/2020 - 23/01/2023	03/01/2020 - 30/04/2023	07/04/2023 - 30/04/2023	18/02/2023 - 30/04/2023	01/01/2020 - 30/04/2023

CCAM-CABLE description

This model consists of two main components, namely the conformal-cubic atmospheric model (CCAM) developed by the Commonwealth Scientific and Industrial Research Organisation (CSIRO) in Australia and a dynamic land-surface model CABLE (CSIRO Atmosphere Biosphere Land Exchange). The model does have a global ocean component developed by CSIRO; however, the simulations undertaken for this project did not use the ocean component, and therefore the focus is on CCAM-CABLE. As a global climate model, CCAM can operate in variable resolution mode, enabling it to function as a regional climate model (Engelbrecht et al., 2009). This allows the model to be run with a high horizontal resolution over the region of interest, with the resolution gradually decreasing as it moves away from this area (Engelbrecht et al., 2011). A key benefit of the variable resolution approach, compared to the traditional nested limited-area modelling, is its increased flexibility in dynamically downscaling from any global model. It primarily requires sea surface temperature and sea-ice data from the host model, avoiding issues such as boundary reflections that can arise in limited-area models. CCAM is based on a quasi-uniform grid, created by projecting the panels of a cube onto the Earth's surface (for a detailed description, see Engelbrecht et al., 2009).

Several studies have used CCAM for climate change projections. For example, Bopape et al. (2022) examined the performance of CCAM in simulating high-impact weather events, with a focus on rainfall predictions in South Africa, and found that CCAM can represent the spatial distribution of rainfall associated with each of the high impact events. Engelbrecht et al. (2011) applied CCAM across a wide range of spatial and time scales and discovered that the model can be successfully applied for extended simulations of present-day climate at spatial scales ranging from global simulations with relatively low horizontal resolution to micro-scale simulations with ultra-high resolution. The CCAM-CABLE model has been tested and developed extensively for application in southern Africa, and more broadly in Africa, over a period of two decades (e.g. Engelbrecht et al., 2019).

ERA5 is the latest reanalysis product from the European Centre for Medium-Range Weather Forecasts (ECMWF). This is a commonly used dataset that has been shown to accurately capture the spatial patterns of rainfall over Africa, although some biases exist (Steinkopf and Engelbrecht, 2022). ERA5 combines observational data (ground observations and satellite data) with a numerical weather prediction model (Dee et al., 2011; Hersbach et al., 2020) to simulate past climate conditions. Therefore, it is often used to verify GCM/RCM outputs. However, this reanalysis dataset is available at a horizontal resolution of 30km. To test how well CCAM simulates land-atmosphere interactions, CCAM-CABLE is used to dynamically downscale

ERA5 over the southern African domain to a horizontal resolution of 8km. That is, in these simulations, the model is nudged within the ERA5 reanalysis data for the period 1979-2021, thereby forcing the simulations to be consistent with historical weather patterns. From this, data at the grid box/pixel associated with each of the corresponding flux tower locations was extracted and compared to the observational data from the flux towers. It is important to note that two of the towers fell within the same 8km pixel and are therefore compared against the same CCAM outputs. This highlights a potential shortcoming of using data at a resolution of 8km, compared to point data (i.e., the flux towers).

Eddy covariance technique and data

The fluxes of carbon dioxide, water vapour, latent heat, and sensible heat between the earth's surface and the atmosphere were measured using the Eddy Covariance (EC) technique. This technique is based on measurements of a gas of interest (CO_2) in the constant flux zone of the surface boundary layer, as well as the fluctuating components of vertical wind (Baldocchi, 2003; Foken and Wichura, 1996). Several data inputs are needed to compute sensible heat, latent heat, carbon, and water fluxes. These include air temperature and pressure, three-dimensional wind speeds, and densities of CO_2 and H_2O. The fluxes were measured at various heights across all the sites using a Campbell Scientific IRGASON® Integrated CO_2/H_2O Open-Path Gas Analyzer and 3D Sonic Anemometer (Campbell Scientific Instruments, Logan, Utah, United States) at a frequency of between 10 - 20 Hz.

At EC flux towers, soil moisture is measured with dielectric probes - typically with time-domain reflectometry (TDR) or capacitance/FDR sensors - at one or more depths within the tower's flux footprint, reporting volumetric water content (%) at 30-minute intervals. Sensors are site-calibrated (soil texture/temperature), and the data are aggregated as depth profiles or depth-weighted averages.

Eddy Covariance Data Processing

The dataloggers from each site were programmed to store and process raw 10-20 Hz data and compute turbulent fluxes at 30-minute averages which were used for analysis. There are certain limitations when using the EC technique in terms of quality control procedures and data processing. This is especially difficult in complex environments with turbulence, poor wind speed, and uneven terrain. Thus, EC data often requires a series of corrections and data processing steps as well as quality control – these steps were all included in the program to suit the various site conditions and instrumentation setups. The Foken et al. (2012) quality control and flagging methodology was applied to all fluxes. These flux correction steps resulted in half-hourly values of CO_2 fluxes or NEE. For the sites used in the study, values outside of the instrument range were filtered out by establishing minimum and maximum thresholds for particular variables. Data marked as good quality (0–4) according to the Foken et al. (2012) quality flagging technique were used for further analysis, while the other data were discarded. For soil moisture, data was aggregated as depth profiles, expressed in volumetric water content (%) at a depth of 2.5 cm to match the soil moisture depths of CCAM and the satellite data.

Earth observation data

Soil moisture

Soil moisture data from the NASA Soil Moisture Active Passive (SMAP) Level 4 Surface and Root Zone Soil Moisture (SPL4SMGP), Version 7 data (Reichle et al. 2022) available in Google Earth Engine (GEE), were used. This dataset provides daily soil moisture estimates at approximately 9 km spatial resolution, generated by assimilating satellite observations into a land surface model.

For each of three flux tower sites, BNK, BSV, and CP, surface soil moisture (0-5 cm) data were extracted. Each site location point was buffered with a 4 km radius to create zones for spatial averaging of the data to match the 8km pixel size of CCAM. Due to the high quality and pre-processed nature of SMAP Level 4 data, no additional quality filtering was performed. However, only images intersecting the buffered points were retained to avoid null outputs.

Above-ground biomass

We used an open-access, global annual above-ground biomass (AGB) time series derived from SMOS L-band vegetation optical depth (L-VOD) (Boitard et al. 2025). This option was selected as we did not have the capacity to process the original product with validation field data. The data from Boitard et al. (2025) were produced using an approach that averages L-VOD by year and calibrates a single global VOD-AGB relationship against an existing AGB reference map, merging ascending and descending orbits. The data record spans 2011 onward, yields biomass values up to ~300 Mg ha^{-1}, and, with benchmarking, shows strong consistency with ESA CCI Biomass v5 (mean R = 0.87) while exhibiting somewhat larger interannual variability and slightly lower absolute AGB than some alternatives.

Data analysis: Comparison between CCAM and EC

The cleaned 30-minute EC data were aggregated to hourly timestamps to align with CCAM hourly timeseries data for the available data periods. Subsequently, the openair R package was used to calculate diurnal means across each variable for each month, followed by monthly and interannual means. To statistically compare CCAM and EC data, the coefficient of determination (R^2), residual standard error (RSE), and percentage bias were computed to evaluate the performance of CCAM outputs versus EC in situ data. All analyses were performed using R statistical software version 4.2.3 (R Core team, 2023).

Data analysis: Comparison between CCAM and EO data

Soil moisture data from EC flux, SMAP and CCAM for three flux tower sites, including BNK, BSV and CP, were aggregated into monthly data. For every pair of time series data, we quantified association and agreement using Pearson correlation (*r*) and R^2, error metrics (RMSE, MAE), level differences (Bias and percent Bias), and performance indices that account for correlation, bias, and variability (Nash–Sutcliffe Efficiency, Kling–Gupta Efficiency, and Lin's concordance correlation coefficient). We also computed discrete cross-correlations over ±6 months to test for lead/lag and generated Bland–Altman plots to visualise systematic and random differences. To separate long-term drift from co-variability, we repeated the analysis

on detrended versions of each time series (linear least-squares trend removed while preserving the mean). Detrending preserves the mean but removes a linear trend component, emphasizing pattern co-variability.

For noise-aware skill estimates independent of any single "truth," we applied triple collocation (TCA) to monthly anomalies (month-of-year climatology removed) and, where possible, to anomalies plus detrending; this yields each data source's error variance, signal-to-noise ratio (SNR), and correlation to an unknown truth (ρ truth) under the standard assumptions of linearity and mutually independent errors. Correlation *p*-values were adjusted using an effective sample size based on lag-1 autocorrelation.

We compiled annual above-ground biomass (AGB) rasters (2014–2023) and annual aggregated CCAM NEE rasters for the same period. For each year, AGB was projected to the WGS84 geographic projection and resampled with bilinear interpolation onto the exact NEE grid to ensure pixel size and origin aligned. The rasters were then clipped and masked to the valid-data footprint of both AGB and NEE to ensure pixel-wise comparability. NEE layers were scaled by 10 000 (for readability) and sign-flipped to NEP (NEP = −NEE) for interpretation (positive = net carbon gain). Per-pixel biomass change was computed as $\Delta AGB = AGB_t - AGB_{t-1}$, yielding a 2015–2023 series for temporal tests. All operations were performed in R.

We ran two complementary correlation analyses. First, we did a spatial cross-sectional correlation per year, and secondly, a temporal (within-pixel) correlation across years (i.e. Pearson correlations of NEP vs ΔAGB). Pixels were reported in the output spatial map only if they had a minimum number of valid annual pairs (default ≥5). Two-sided p-values were obtained from the correlation t-statistic and adjusted for multiple testing using Benjamini–Hochberg FDR, yielding q-value maps and significance masks ($q \leq 0.05$ and 0.10).

Results

CCAM comparisons to EC

Monthly comparison between CCAM and EC

Net Ecosystem Exchange

A monthly comparison of the Net Ecosystem Exchange (NEE) is compared between CCAM and EC, across the various sites, to examine the seasonal cycle (Figure 1). CCAM consistently underestimates CO_2 uptake periods across all months and at all sites, except for CP where there is an overestimation between August and December (Figure 1). According to observations, the first three months act as a sink, becoming neutral from May to August and returning to sink thereafter at BSV, BNK and CP. JHK remains a sink throughout the year. In contrast, CCAM indicates all sites acting as a source throughout the year, except at CP, where it only becomes a source between August and November (Figure 1). CCAM-EC correlations are weak, with CCAM outputs explaining between 1% (at BSV) and 11% (at BNK) of NEE variability (Figure 2).

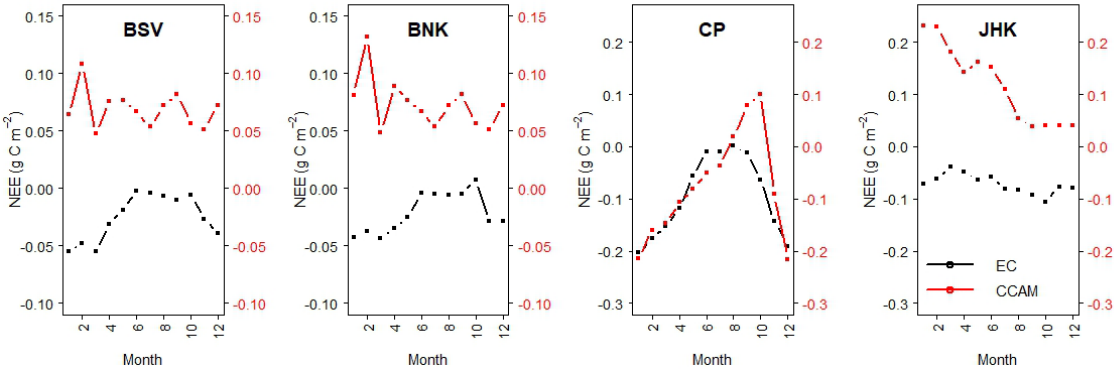

Figure 1: Monthly means of Net Ecosystem Exchange from Eddy Covariance data versus CCAM outputs at Benfontein Savanna (BSV), Benfontein Nama-Karoo (BNK), Cathedral Peak (CP) and Jonkershoek (JHK) EFTEON sites.

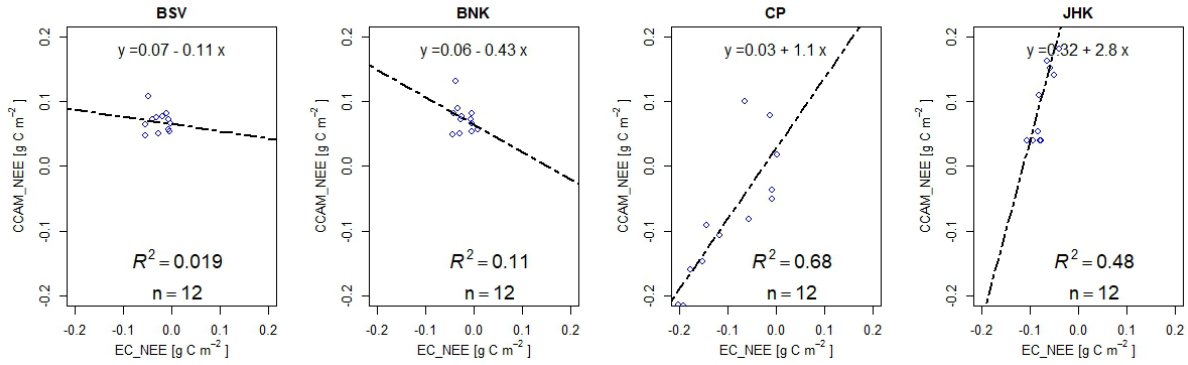

Figure 2: Scatterplot diagrams showing the relationship between CCAM and EC measured Net Ecosystem Exchange at the monthly timescale across four EFTEON sites.

Latent Heat

Considering the seasonal cycle of Latent Heat (LE), similar patterns are observed at the BSV, BNK and CP sites, with both EC and CCAM peaking during the summer months and lowest during the winter months (Figure 3). CCAM consistently underestimates the magnitude of the peaks during the summer months. At JHK, CCAM gets a similar seasonal cycle to EC, but severely underestimates LE fluxes, remaining below 50 throughout the year, while EC measurements range between 100 and 150 (Figure 3). CCAM-EC correlations are strong for BSV (R^2 = 0.93), BNK (R^2 = 0.84), and CP (R^2 = 0.91), but a weak correlation is found at JHK (R^2 = 0.23) (Figure 4). Overall, CCAM consistently underestimates LE throughout the year.

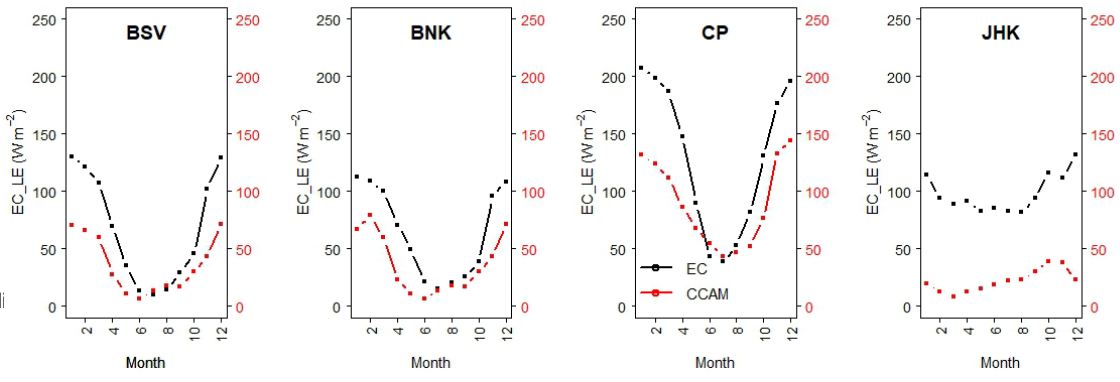

Figure 3: Monthly means of Latent Heat from Eddy Covariance data versus CCAM outputs at Benfontein Savanna (BSV), Benfontein Nama-Karoo (BNK), Cathedral Peak (CP) and Jonkershoek (JHK) EFTEON sites.

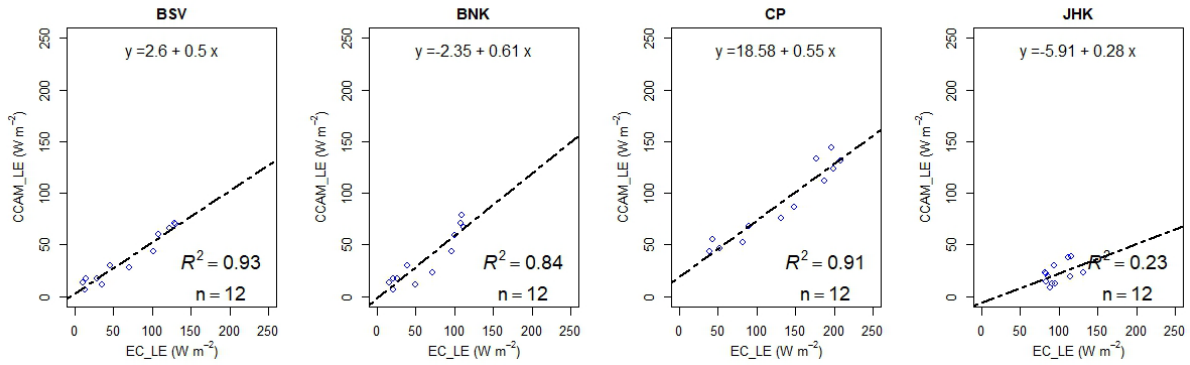

Figure 4: Scatterplot diagrams showing the relationship between CCAM and EC measured Latent Heat at the monthly timescale across four EFTEON sites.

Sensible Heat

Figure 5 shows the monthly comparison of Sensible Heat (H) as estimated by CCAM and measured by EC, across the four sites. BSV and BNK exhibit almost identical cycles in the observed H fluxes, with CCAM displaying a much stronger seasonal cycle at both sites, overestimating during the summer months and underestimating during the winter months (Figure 5). At CP, CCAM consistently underestimates H fluxes throughout the year and reverses the seasonal cycle completely, peaking during summer months instead of winter months. It is notable that CP is the only site at which EC shows high H during the winter months. At JHK, CCAM does well at capturing the seasonal cycle, overestimating the peak during January-February and October-December (Figure 5). CCAM-EC correlations are weak at BSV (R^2 = 0.32), BNK (R^2 = 0.21) and CP (R^2 = 0.32), but strong at JHK (R^2 = 0.9) (Figure 6).

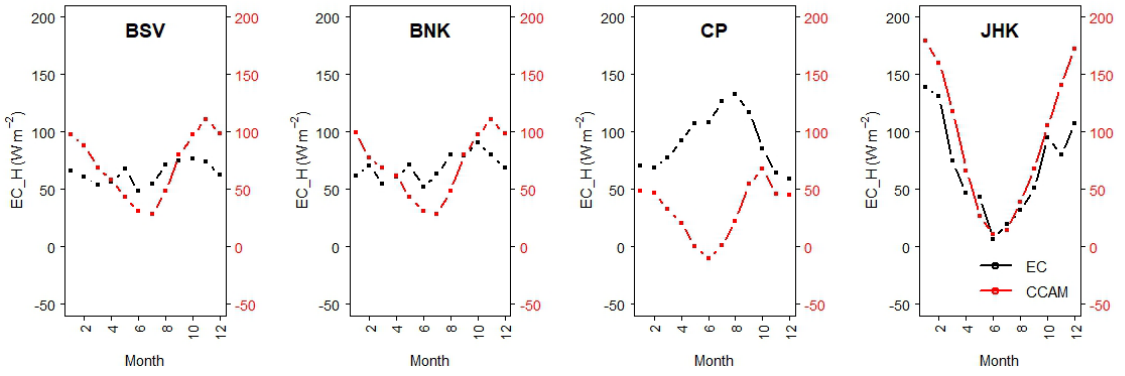

Figure 5: Monthly means of Sensible Heat from Eddy Covariance data versus CCAM outputs at Benfontein Savanna (BSV), Benfontein Nama-Karoo (BNK), Cathedral Peak (CP) and Jonkershoek (JHK) EFTEON sites.

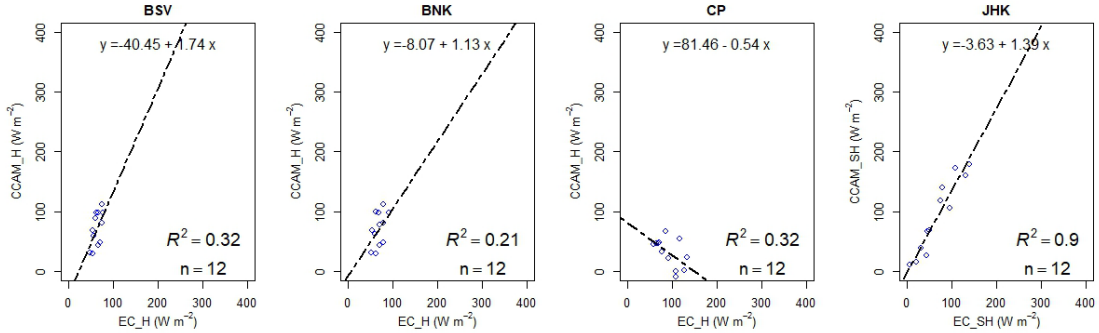

Figure 6: Scatterplot diagrams showing the relationship between CCAM and EC measured Sensible Heat at the monthly timescale across four EFTEON sites.

Diurnal comparison between CCAM and EC

Net Ecosystem Exchange

The diurnal cycle of the Net Ecosystem Exchange (NEE) is compared between CCAM and EC, across the various sites, during both wet and dry seasons (Figure 7). Across both seasons, the diurnal cycle is well-represented in the CCAM simulations, but CCAM tends to underestimate CO_2 uptake periods, except at the CP site, where it significantly overestimates both daytime and nighttime fluxes (Figure 7). There are notable double peaks in CCAM estimates for the BSV and BNK sites. In the early morning, both act as CO_2 sources, transition to sinks around midday, and revert to sources in the afternoon.

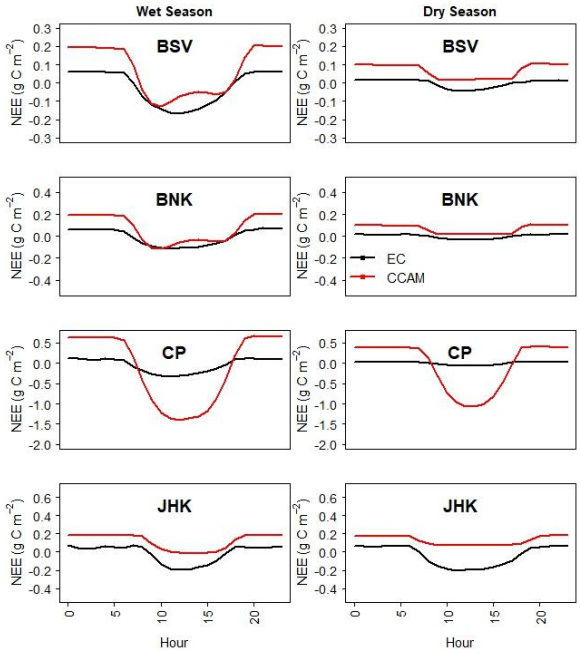

Figure 7: Diurnal patterns of Net Ecosystem Exchange from Eddy Covariance data versus CCAM model outputs at Benfontein Savanna (BSV), Benfontein Nama-Karoo (BNK), Cathedral Peak (CP) and Jonkershoek (JHK) EFTEON sites.

During the dry season, in situ measurements of NEE at the diurnal scale show the BSV, BNK, and CP sites as carbon neutral, with all ecosystems showing less physiological activity compared to the wet season (Figure 7). The JHK site exhibited sink characteristics during the day between the dry months of September to April. What is notable here is that while JHK is located in a winter rainfall region, physiological activity remained relatively similar between both dry and wet seasons, with CCAM underestimating diurnal CO_2 fluxes during both periods, but to a greater extent during the dry season. CCAM-EC correlations are positive and strong, with CCAM outputs explaining between 78% (at JHK) and 92% (at BNK) of NEE variability (Figure 8). Generally, wet season correlations were stronger across the sites, except for CP - with a marginal difference (not shown).

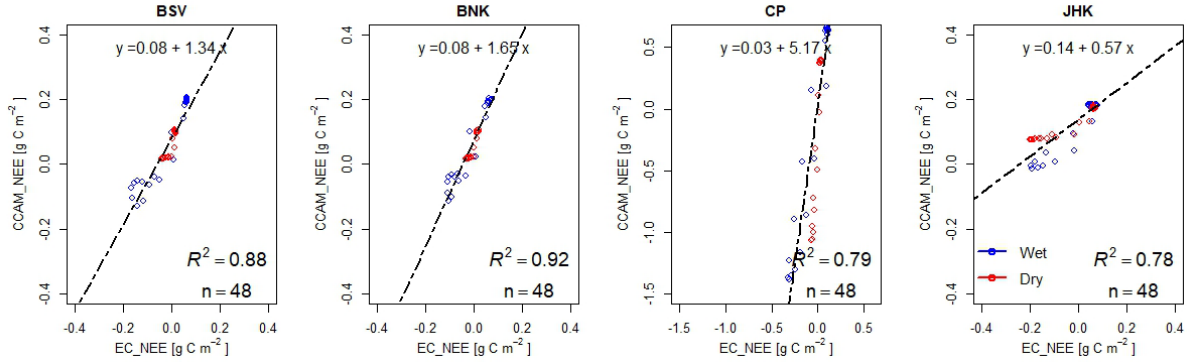

Figure 8: Scatterplot diagrams showing the relationship between CCAM and EC measured Net Ecosystem Exchange at the diurnal scale across four EFTEON sites.

Latent Heat

Considering the diurnal cycle in latent heat (LE) between CCAM and EC, similar patterns emerge in the dry and wet seasons, with low LE in the early hours, followed by an increase through to a midday peak and a subsequent decrease in the afternoon (Figure 9). While CCAM consistency follows the cycle evident in the EC observations, it does underestimate the LE peaks across all sites except the CP site where it overestimates the midday peak, especially in the dry season. The most notable underestimation of daytime and nighttime LE fluxes by CCAM is observed at JHK (Figure 9). CCAM-EC correlations were strong, with CCAM outputs explaining between 83% (at JHK) and 98% (at BNK) of measured LE variability (Figure 10). Generally, wet season correlations were stronger across the sites, except for JHK - with a marginal difference (not shown).

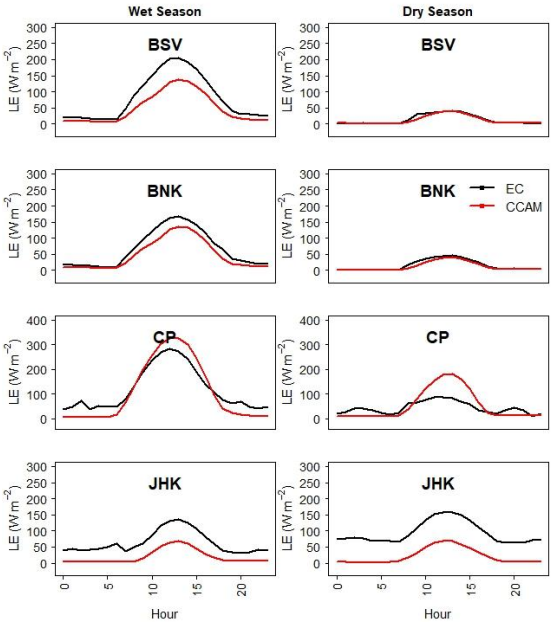

Figure 9: Diurnal patterns of Latent Heat from Eddy Covariance data versus CCAM model outputs at Benfontein Savanna (BSV), Benfontein Nama-Karoo (BNK), Cathedral Peak (CP) and Jonkershoek (JHK) EFTEON sites.

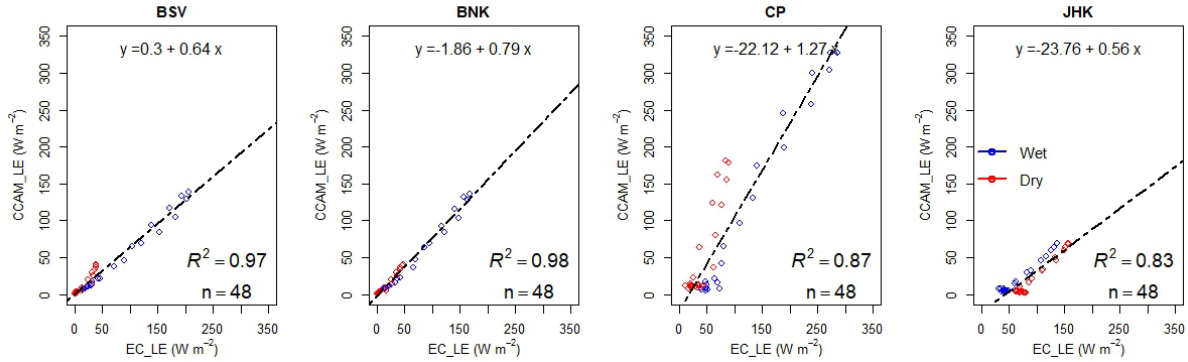

Figure 10: Scatterplot diagrams showing the relationship between CCAM and EC measured Latent Heat at the diurnal scale across four EFTEON sites.

Sensible Heat

Considering the diurnal cycle in sensible heat (H), similar patterns between CCAM and EC were observed in both seasons (Figure 11). For the wet season, CCAM consistently overestimates the peak of H, most notably at the BSV and BNK sites. Interestingly, for the dry season, CCAM is most similar to EC at these two sites, and notably overestimates H fluxes at JHK and underestimates at CP (Figure 11). CCAM-EC correlations were strong, with CCAM outputs explaining between 81% (at CP) and 96% (at BNK) of measured H variability. Correlations were particularly strong at BSV and BNK, with R^2 values of 0.94 and 0.96, respectively (Figure 12). These high correlations together with the lower correlation at the CP site, suggests CCAM was able to

represent the variability of H fluxes better in semi-arid regions compared to wetter sites. Generally, dry season correlations were very marginally stronger across the sites, except for JHK (not shown).

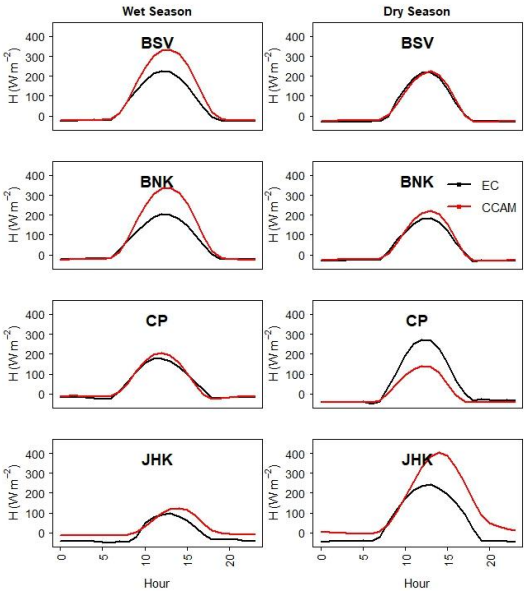

Figure 11: Diurnal patterns of Sensible Heat from Eddy Covariance data versus CCAM model outputs at Benfontein Savanna (BSV), Benfontein Nama-Karoo (BNK), Cathedral Peak (CP) and Jonkershoek (JHK) EFTEON sites.

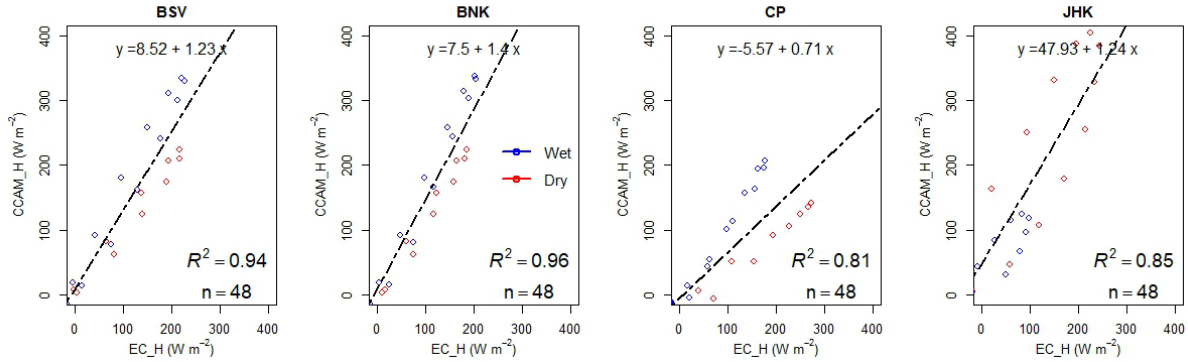

Figure 12: Scatterplot diagrams showing the relationship between CCAM and EC measured Sensible Heat at the diurnal scale across four EFTEON sites.

CCAM Comparison to Earth Observation Data

Monthly comparison of Soil Moisture

In this section, the monthly time series of the soil moisture from SMAP, CCAM and EC is presented together with the regression models.

Benfontein Nama-Karoo

Soil moisture time series comparison (BNK)

From the detrended time series plot (Figure 13), it appears visually that the soil moisture data from EC, SMAP, and CCAM follow a similar seasonal cycle with comparable trends. There are, however, instances where CCAM increases when EC and SMAP decrease, and vice versa. SMAP and CCAM exhibited some differences in magnitude, while both data sources consistently recorded higher estimates of soil moisture than EC.

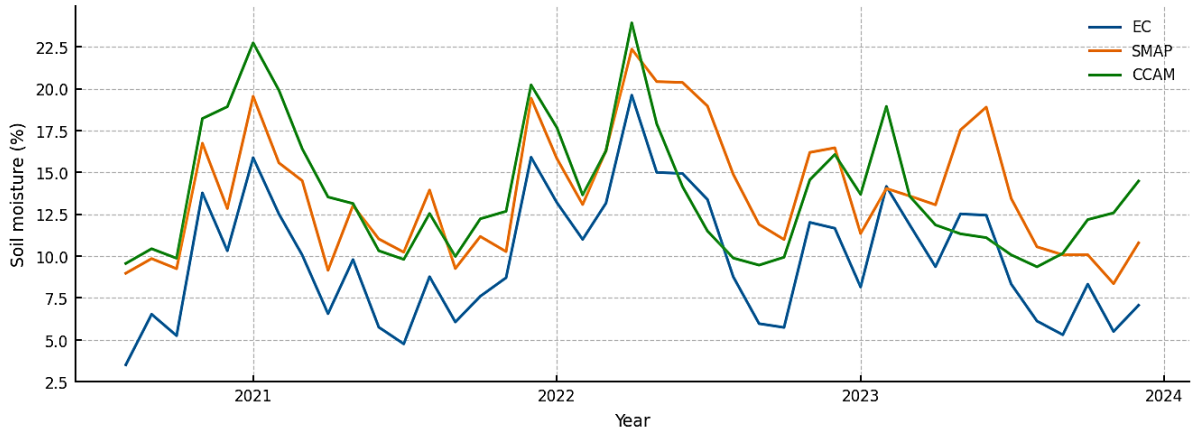

Figure 13. Time series plot of soil moisture (%) estimates from EC flux, SMAP and CCAM at the Benfontein Nama-Karoo flux tower site.

Soil moisture pairwise comparisons (BNK)

The scatterplots of soil moisture from EC, SMAP, and CCAM are presented in Figure 14, and the results of statistical tests are in Table 2. The strongest correlations for all pairwise comparisons occur at 0-month lag, indicating no systematic lead/lag at a monthly resolution.

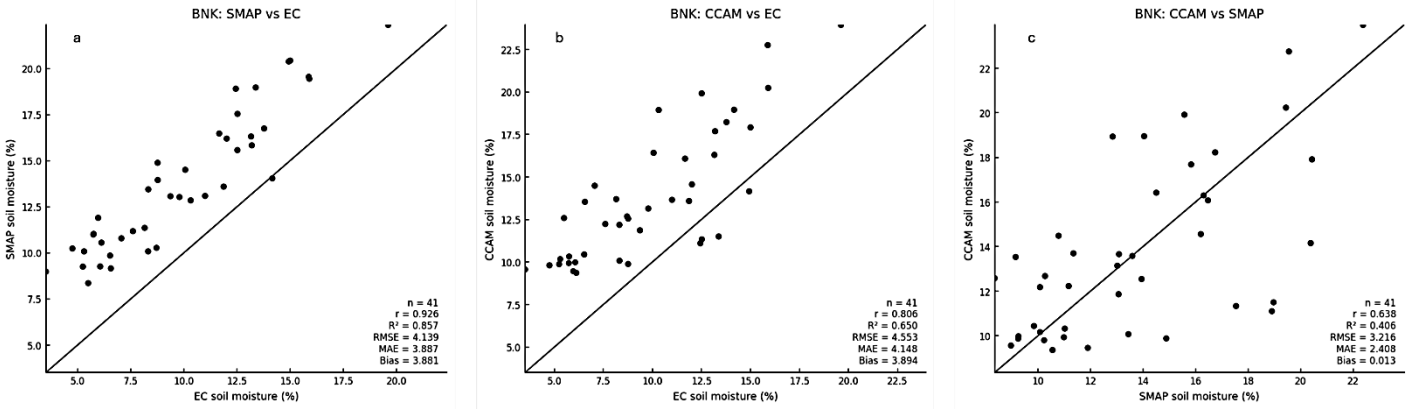

Figure 14. Pairwise comparisons of soil moisture (%) from (a) SMAP to EC, (b) CCAM to EC, and (c) CCAM to SMAP at the Benfontein Nama-Karoo flux tower site.

Table 2. Correlation and agreement metrics for pairwise comparisons between soil moisture from EC, SMAP and CCAM for the Benfontein Nama-Karoo flux tower site

Comparison	Pearson r	R^2	p	RMSE	MAE	Bias	PBIAS %	NSE	KGE	Lin CCC
SMAP - EC (raw)	0.93	0.86	0.72	4.14	3.89	3.88	39.26	-0.22	0.60	0.61
SMAP - EC (detrended)	0.93	0.86	0.72	4.14	3.89	3.88	39.26	-0.22	0.60	0.61
CCAM - EC (raw)	0.81	0.65	0.79	4.55	4.15	3.89	39.39	-0.48	0.56	0.53
CCAM - EC (detrended)	0.83	0.68	0.78	4.47	4.04	3.89	39.39	-0.43	0.57	0.54
CCAM - SMAP (raw)	0.64	0.41	0.86	3.22	2.41	0.01	0.10	0.25	0.64	0.64
CCAM - SMAP (detrended)	0.66	0.44	0.86	3.08	2.29	0.01	0.10	0.32	0.66	0.66

(a) SMAP Vs EC pairwise comparison

Results from statistical analyses reveal a strong linear association (r = 0.93, R^2 = 0.86) between the soil moisture data from SMAP and EC; however, a substantial positive bias (Bias = 3.88; PBIAS = 39%) is observed. Magnitude mismatch drives negative NSE (−0.22) despite good co-variability. KGE = 0.60 and CCC = 0.61 indicate moderate overall agreement, considering bias and variance. After detrending, the correlation remains high (r = 0.93); the RMSE and bias are mostly unchanged, and the KGE is 0.60. This implies most of the SMAP-EC correlation arises from seasonal or interannual variability, rather than a shared trend.

(b) CCAM vs EC pairwise comparison

A strong correlation (r = 0.81, R^2 = 0.65) with a positive bias (Bias = 3.89; PBIAS = 39%) was observed between CCAM and EC soil moisture, consistent with the comparison between SMAP and EC. NSE = −0.48 and KGE = 0.56, showing that scaling differences limit performance relative to EC. The association improves slightly after detrending (r = 0.83, R^2 = 0.68), with the RMSE decreasing slightly from 4.55 to 4.47, and the NSE becoming less negative (−0.43); KGE and CCC remain almost unchanged.

(c) CCAM vs SMAP pairwise comparison

Analyses showed a moderate correlation (r = 0.64, R^2 = 0.41) with negligible bias (Bias = 0.01; PBIAS = 0.1%). NSE = 0.25, KGE = 0.64, CCC = 0.64 suggest that the SMAP and CCAM soil moisture time series track each other's variability reasonably well. After detrending, the correlation strengthens slightly (r = 0.66, R^2 = 0.44), with lower RMSE and NSE rising to 0.32; both KGE and CCC are 0.66. Removing linear drift clarifies shared variability between the two data sets.

(d) Triple collocation on anomalies

The soil moisture time series from EC shows minimal random error and ρ truth = 0.995–0.997 with very high SNR (= 100–143), consistent with EC serving as a strong local reference (in situ) data set. SMAP performs

well (ρ truth = 0.936, SNR = 7), indicating a robust signal with relatively low noise. CCAM exhibits a larger random error with ρ truth = 0.77 (raw anomalies), improving to 0.81 after detrending, with the SNR rising from 1.4 to 1.9. This indicates a meaningful CCAM skill in variability, but with weaker signal strength and some trend or scaling mismatch relative to the others.

Benfontein Savanna

Soil moisture time series comparison (BSV)

From the detrended time series plot (Figure 15), it appears visually that the soil moisture data from EC, SMAP, and CCAM follow a similar seasonal cycle with comparable trends, with some anomalies, similar to those observed at the BNK site. SMAP and CCAM have only slight differences in magnitude, while both data sources consistently recorded higher estimates of soil moisture.

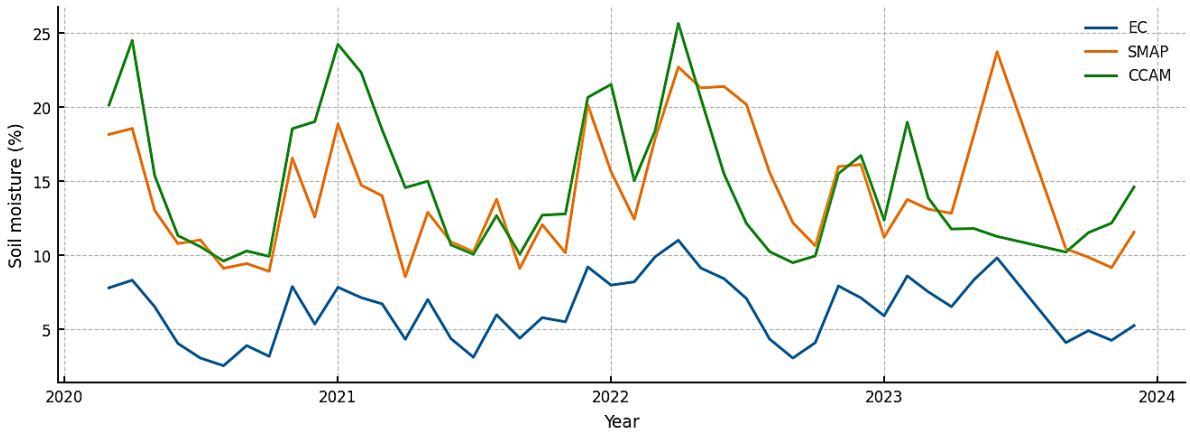

Figure 15. Time series plot of soil moisture (%) estimates from EC flux, SMAP and CCAM at the Benfontein Savanna flux tower site.

Soil moisture pairwise comparisons (BSV)

The scatterplots of soil moisture from EC, SMAP and CCAM are shown in Figure 16, and the results of statistical tests are presented in Table 3. Similar to the BNK site, the strongest correlations for all pairwise comparisons occur at 0-month lag, indicating no systematic lead/lag at a monthly resolution.

(a) SMAP vs EC comparison

The correlation between soil moisture data from SMAP and EC showed a strong linear association (r = 0.85, R^2 = 0.72), but a significant positive bias (Bias = 7.77; PBIAS = 123%). With NSE = −13.56, KGE = −0.55, and CCC = 0.19, significant magnitude differences were observed. After detrending, the SMAP-EC correlation remained unchanged, and the strong positive bias, indicating a magnitude mismatch, persisted (NSE = −14.02, KGE = −0.56, CCC = 0.18).

(b) CCAM vs EC comparison

CCAM soil moisture estimates showed a moderate correlation with the EC soil moisture (r = 0.730, R^2 = 0.534), but with significant positive bias (Bias = 8.53; PBIAS = 136%). Similar to the SMAP-EC comparison, agreement metrics reflect a scaling issue: NSE = −17.24, KGE = −0.780, CCC = 0.15. Detrending improved the correlation (r = 0.804, $R^2 \approx 0.647$), but the magnitude mismatch remains.

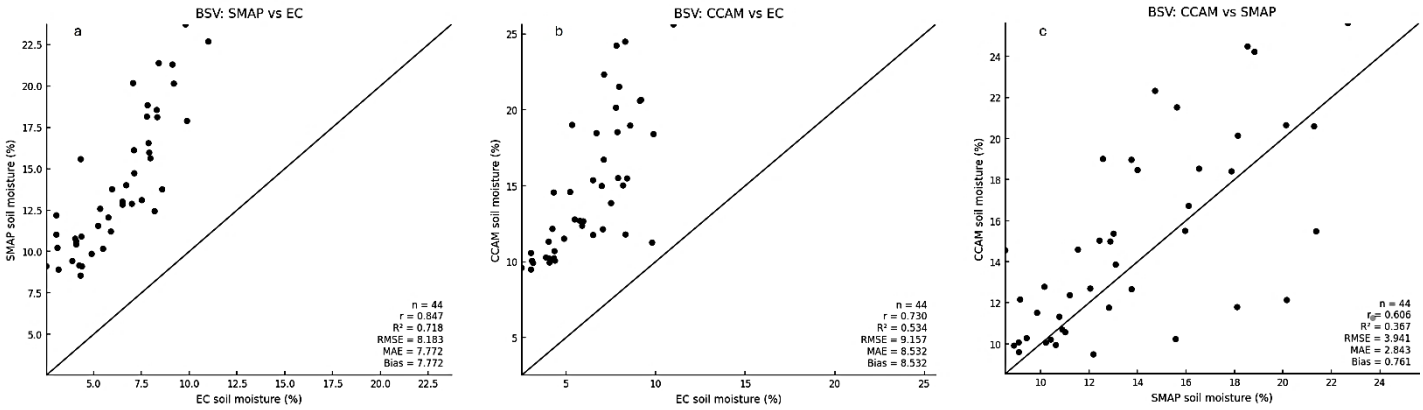

Figure 16. Pairwise comparisons of soil moisture (%) from (a) SMAP to EC, (b) CCAM to EC, and (c) CCAM to SMAP at the Benfontein Savanna flux tower site.

Table 3. Correlation and agreement metrics for pairwise comparisons between soil moisture from EC, SMAP and CCAM for the Benfontein Savanna flux tower site.

Comparison	Pearson r	R^2	p	RMSE	MAE	Bias	PBIAS%	NSE	KGE	Lin CCC
SMAP vs EC (raw)	0.847	0.718	0.797	8.183	7.772	7.772	123.45	-13.564	-0.546	0.186
SMAP vs EC (detrended)	0.846	0.716	0.801	8.183	7.772	7.772	123.45	-14.015	-0.557	0.182
CCAM vs EC (raw)	0.73	0.534	0.83	9.157	8.532	8.532	135.53	-17.237	-0.78	0.148
CCAM vs EC (detrended)	0.804	0.647	0.803	9.046	8.532	8.532	135.53	-17.35	-0.754	0.158
CCAM vs SMAP (raw)	0.606	0.367	0.879	3.941	2.843	0.761	5.41	0.082	0.588	0.594
CCAM vs SMAP (detrended)	0.652	0.425	0.868	3.647	2.799	0.761	5.41	0.204	0.638	0.64

(c) SMAP vs CCAM comparison

A moderate association (r = 0.606, R^2 = 0.367) was found between SMAP and CCAM, with small positive bias (Bias = 0.76; PBIAS = 5.4%), while the magnitude and scaling agreement were reasonable (NSE = 0.082, KGE = 0.588, CCC = 0.59). The correlation improved slightly in the detrended data (r = 0.652, R^2 = 0.425), while removing linear drift clarifies shared variability between the two data sets.

(d) Triple collocation (monthly anomalies)

Considering the raw anomalies, TCA produced inconsistent values for SMAP (ρ truth > 1, negative SNR), indicating numerical instability at BSV, likely due to the very large inter-time series mean and variance differences. However, once trends were removed, SMAP has a strong SNR for variability, while CCAM has a meaningful but weaker intrinsic skill (EC: ρ truth = 0.906, SNR = 4.60; SMAP: ρ truth = 0.982, SNR = 27.20; CCAM: ρ truth = 0.791, SNR = 1.68), resulting in the ranking; SMAP > EC > CCAM by SNR; EC ≈ SMAP > CCAM (by ρ truth).

Cathedral peak

Soil moisture time series comparison (CP)

From the detrended time series plot (Figure 17), it appears visually that the soil moisture data from EC, SMAP and CCAM generally follow the seasonal cycle trend. SMAP and CCAM differed in magnitude, with both consistently showing much lower estimates of soil moisture than EC.

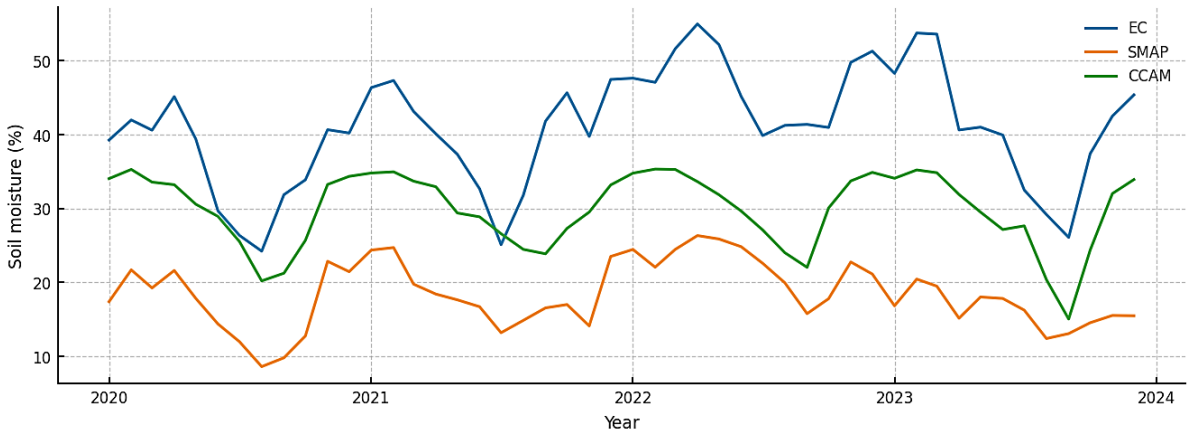

Figure 17. Time series plot of soil moisture (%) estimates from EC flux, SMAP and CCAM at the Benfontein Nama-Karoo flux tower site.

Soil moisture pairwise comparisons (BNK)

The scatterplots of soil moisture derived for EC, SMAP and CCAM at the CP flux tower site are presented in Figure 18, and the results of statistical tests are in Table 4. The strongest correlations for all pairwise comparisons occur at 0-month lag, indicating no systematic lead/lag at a monthly resolution

(a) SMAP vs EC comparison

For the comparison between SMAP and EC, the results show a strong association (r = 0.791, R^2 = 0.626) but a substantial negative bias (Bias ≈ −22.51; PBIAS ≈ −55%), indicating that SMAP observations of soil moisture are, on average, much lower than those of EC. A magnitude mismatch is evident, with NSE = −7.829, KGE = 0.264, and CCC = 0.092. After detrending, the correlation slightly increases (r = 0.817) but the magnitude metrics remain poor (NSE = −8.259, KGE = 0.280, CCC = 0.093).

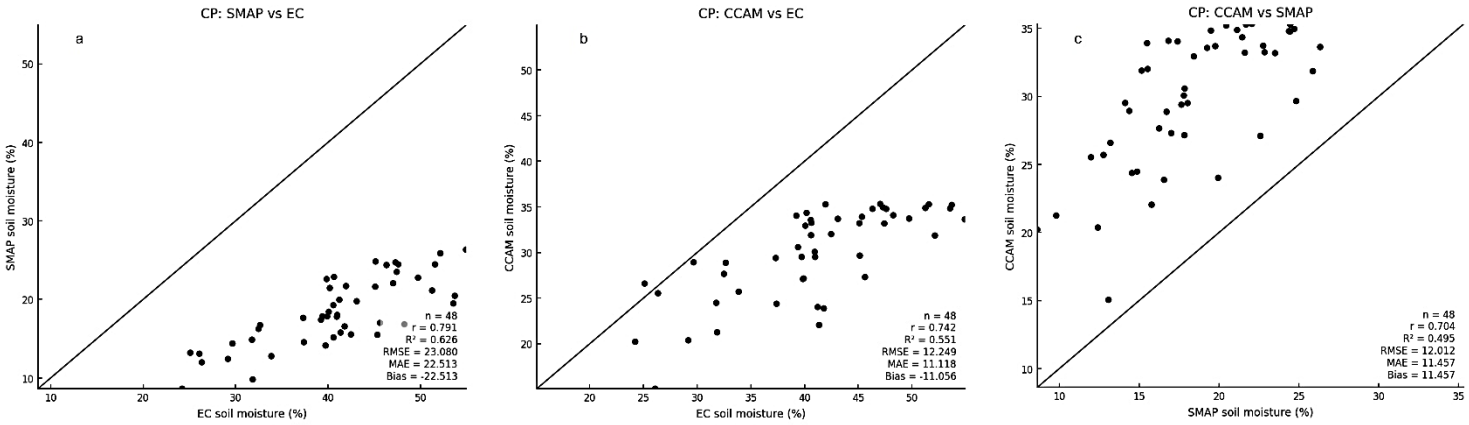

Figure 18. Pairwise comparisons of soil moisture (%) from (a) SMAP to EC, (b) CCAM to EC, and (c) CCAM to SMAP at the Benfontein Savanna flux tower site.

Table 4. Correlation and agreement metrics for pairwise comparisons between soil moisture from EC, SMAP and CCAM for the Cathedral Peak flux tower site.

Comparison	Pearson r	R^2	p	RMSE	MAE	Bias	PBIAS %	NSE	KGE	Lin CCC
SMAP - EC (raw)	0.791	0.626	0.743	23.080	22.513	-22.513	-55.01	-7.829	0.264	0.092
SMAP - EC (detrended)	0.817	0.667	0.73	23.006	22.513	-22.513	-55.01	-8.259	0.28	0.093
CCAM - EC (raw)	0.742	0.551	0.758	12.249	11.118	-11.056	-27.01	-1.487	0.478	0.278
CCAM - EC (detrended)	0.802	0.642	0.728	12.001	11.077	-11.056	-27.01	-1.52	0.513	0.295
CCAM - SMAP (raw)	0.704	0.495	0.792	12.012	11.457	11.457	62.22	-6.694	0.297	0.175
CCAM - SMAP (detrended)	0.708	0.501	0.791	11.998	11.457	11.457	62.22	-6.677	0.301	0.175

(b) CCAM vs EC comparison

Soil moisture from CCAM showed a moderate correlation with EC (r = 0.742, R^2 = 0.551), but with an additional negative bias (Bias = −11.06; PBIAS = −27%) and a magnitude mismatch (NSE = −1.487, KGE = 0.478, CCC = 0.278). Detrending improved the correlation (r = 0.802, R^2 = 0.642), but the bias remains (Bias = −11.06, NSE = −1.520, KGE = 0.513, CCC = 0.295).

(c) CCAM vs SMAP comparison

Comparison of CCAM with SMAP showed a relatively strong correlation (r = 0.704, R^2 = 0.495) and positive bias (Bias = +11.46; PBIAS = +62%), with CCAM estimating higher soil moisture than SMAP on average (NSE = −6.694, KGE = 0.297, CCC = 0.175). Detrending showed very slight, but negligible improvement (r = 0.708; NSE = −6.677, KGE = 0.301, CCC = 0.175).

(d) Triple collocation (monthly anomalies)

At CP, the raw-anomaly results show that EC tracks the truth most closely (ρ = 0.890) with a comparatively strong signal-to-noise ratio (SNR = 3.80), outperforming SMAP (ρ = 0.790; SNR = 1.66) and CCAM (ρ = 0.632; SNR = 0.67), hence the intrinsic variability skill ranks EC > SMAP > CCAM. After detrending, EC's relationship to truth sharpens markedly (ρ = 0.990) and its SNR increases to 49.07, indicating that removing drift eliminates much of the noise in the EC series. In contrast, SMAP and CCAM show only modest gains (SMAP: ρ = 0.749, SNR = 1.28; CCAM: ρ = 0.685, SNR = 0.88), suggesting that their intrinsic signal-to-noise remains limited even after drift removal.

Spatial comparison of Biomass to CCAM NEE

The spatial correlation over annual time steps between NEP and ΔAGB shows limited evidence for a meaningful spatial relationship (Figure 19). Only ± 33% of pixels had enough non-missing years to compute a correlation, and the average temporal depth per pixel was just 3 years. With such short series, correlations are inherently noisy and under-powered. The average effect was a very weak positive association (mean r = 0.10; median r = 0.098), suggesting that years with greater net carbon gain tend to coincide with slightly higher biomass increments. After controlling for multiple testing (FDR), no pixels remained significant ($q \leq 0.05$ or $q \leq 0.10$), which is expected given the short record and small effect sizes.

By contrast, the spatial (cross-sectional) analysis across pixels within each year is better powered. Over 10 years (2014–2023), the weighted mean correlation between NEP and AGB is small and negative (mean = −0.094; median = −0.043), with annual values ranging from a moderate negative (−0.51) to almost zero (−0.004).

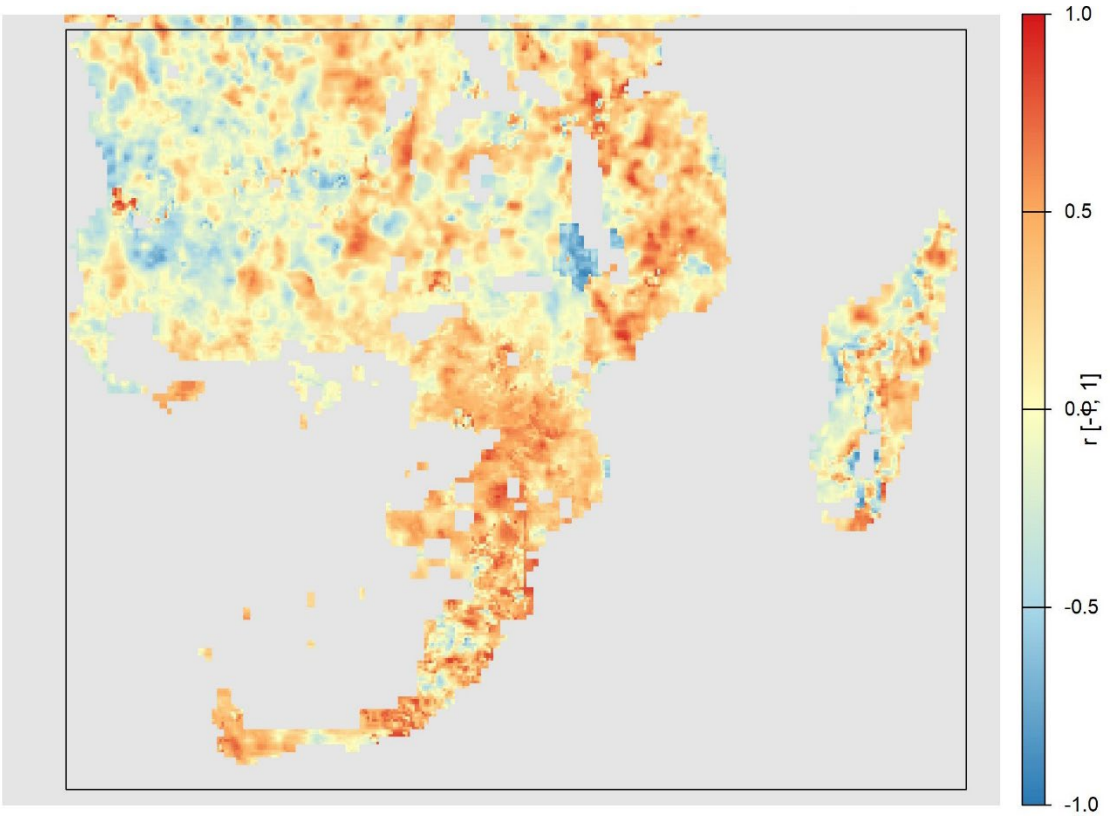

Figure 19. A map showing the per-pixel Pearson temporal correlation (r) between NEP and ΔAGB for 2015–2023. Warm colours (yellow to red) indicate positive correlations - years with higher net carbon gain tended to coincide with biomass increases - while cool colours (light to dark blue) indicate negative correlations.

Concluding Remarks

While the African-based ESM with CCAM and CABLE as primary components has been widely used in various studies around the globe, there are far less studies that have looked at the validation of the model over the African domain. This may partly be driven by the lack of available and reliable observational data sets and the sparse network of in situ measurements across the continent. Modelled data continues to be an integral part of understanding vital ecosystem processes, particularly for water-limited ecosystems where the role of water is pronounced in limiting ecosystem production and sink strength. This remains a critical focus for southern African earth systems science over the next few decades and has been reflected in the establishment of the Expanded Freshwater and Terrestrial Environmental Observation Network (EFTEON), which aims to set up observation systems for ecosystem functioning in various South African biomes. This network provides an invaluable opportunity to validate the CCAM-centred ESM in terms of its representation of land-atmosphere fluxes, which is presented here. The outputs for this validation will inform improvements of the parameterization of land-surface attributes in the CCAM-CABLE ESM.

The comparison of Net Ecosystem Exchange (NEE) between CCAM modelled outputs and EC measurements reveals that CCAM consistently underestimates CO_2 uptake at three of the four examined

EFTEON sites (Benfontein Savanna (BSV), Benfontein Nama-Karoo (BNK) and Jonkershoek (JHK)) across all months. At the Cathedral Peak (CP) site, CCAM overestimates uptake from August to December. Observations indicate that seasonal shifts occur between sink and neutral states at most sites, whereas CCAM incorrectly simulates a continuous CO_2 source, except at CP. These findings are consistent with the diurnal cycle analysis, in which CCAM underestimates CO_2 uptake at BSV, BNK and JHK throughout the day, in both the wet and dry seasons. For CP, CCAM overestimates uptake in both the wet and dry seasons during the midday hours. For Latent Heat (LE), CCAM captures the seasonal cycle at most sites but underestimates summer peaks, particularly at JHK, where it remains significantly lower than EC values throughout the year. This is consistent with the diurnal analysis, which showed CCAM consistently underestimating LE throughout the day, particularly during the wet season, but for both seasons at JHK.

Sensible Heat (H) fluxes exhibit varying biases, with CCAM overestimating summer values at BSV and BNK, reversing the seasonal cycle at CP, and closely matching JHK except for peak overestimations. At CP, CCAM closely matches EC measurements of H fluxes in the summer months, which is supported by the strong correlations in the diurnal cycle during the wet season. However, CCAM significantly underestimates the peak in H between 10h00 and 15h00 during the dry season, likely driving the very low estimations noted in the winter months. Although some biases are evident in the CCAM-CABLE representation of land-atmosphere fluxes, overall, the ESM does exceptionally well at capturing the key characteristics. Additionally, the skill of the model varies by site. For example, CCAM was able to represent the variability of H fluxes better in semi-arid regions compared to wetter sites.

Across all three sites, CCAM and SMAP captured the monthly soil-moisture variability seen in EC reasonably well ($r = 0.64–0.93$), but both exhibit significant, site-dependent magnitude biases relative to EC. At BNK and BSV, SMAP and CCAM are positively biased, while negatively biased at CP. These biases can be ascribed to scaling mismatches. Detrending nudges r upward but does not correct bias, implying that seasonality is captured well, but the absolute values of soil moisture are not.

SMAP and CCAM soil moisture observations agree moderately with each other ($r = 0.60–0.71$), with low bias at BNK and BSV, but a large positive CCAM bias at CP (+62% vs SMAP). Triple-collocation on monthly anomalies consistently ranks EC as the strongest truth-like reference, as expected, followed by SMAP, and then CCAM. CCAM showed the weakest intrinsic variability. However, even with the scale mismatch, CCAM can track variability of soil moisture. This provides a solid base from which comparisons with satellite data can be refined and used for calibrating CCAM to enable comparisons of soil moisture magnitude.

Linking remotely sensed biomass to the CCAM NEE, Figure 19 shows a weak, non-significant positive tendency. This is not surprising, given the short per-pixel record (3 years), which would make it difficult to account for any lag between NEP and structural growth. In contrast, spatial NEP - AGB correlations are small and slightly negative in most years, consistent with vegetation age and structure effects. For instance, high-AGB, respiration-dominated vegetation stands tend to lower NEP. Moreover, since we did not have data to account for plant or soil respiration, the carbon flux, as measured by NEE, could not be closed, as carbon stock presents only one component of the flux. Future work will include addressing scaling mismatches, increasing field data for validation and calibration, and integrating more flux components to better represent the flux.

The research presented in this report highlights the importance of undertaking such a validation across various spatial domains. The results in this investigation will have important implications for improving the parameterizations of land-surface attributed within the model. Additionally, further validation against remote sensing data will be undertaken to better understand the biases evident in the model. This work serves as a blueprint for the identification and reduction of key biases in ESM land-surface and land-atmosphere flux attributes in Africa, towards application in the larger set of Coupled Model Intercomparison Project (CMIP) ESMs, which provide many climate services.

References

Ahlström, A. et al., 2015. The dominant role of semi-arid ecosystems in the trend and variability of the land CO2 sink. Science 348,895-899. https://doi.org/10.1126/science.aaa1668

Archibald, S.A., Kirton, A., Van der Merwe, M.R., Scholes, R.J., Williams, C.A. and Hanan, N., 2009. Drivers of inter-annual variability in Net Ecosystem Exchange in a semi-arid savanna ecosystem, South Africa. *Biogeosciences*, *6*(2), pp.251-266. https://doi.org/10.5194/bg-6-251-2009.

Baldocchi, D.D., 2003. Assessing the eddy covariance technique for evaluating carbon dioxide exchange rates of ecosystems: past, present and future. *Global change biology*, *9*(4), pp.479-492. https://doi.org/10.1046/j.1365-2486.2003.00629.x.

Bonan, G. B., and Doney, S. C., 2018. Climate, ecosystems, and planetary futures: The challenge to predict life in Earth system models. *Science*, *359*(6375). https://doi.org/10.1126/science.aam8328.

Bopape, M. J. M., Engelbrecht, F. A., Maisha, R., Chikoore, H., Ndarana, T., Lekoloane, L., Thatcher, M., Mulovhedzi, P. T., Rambuwani, G. T., Barnes, M. A., Mkhwanazi, M., & Mphepya, J., 2022. Rainfall Simulations of High-Impact Weather in South Africa with the Conformal Cubic Atmospheric Model (CCAM). *Atmosphere*, *13*(12), 1–24. https://doi.org/10.3390/atmos13121987.

Chen, F., Crow, W. T., Bindlish, R., et al. (2018). Global-scale evaluation of SMAP, SMOS and ASCAT soil moisture products using triple collocation. *Remote Sensing of Environment*, 214, 1–13. https://doi.org/10.1016/j.rse.2018.05.008

Collins, W. J., Bellouin, N., Doutriaux-Boucher, M., Gedney, N., Halloran, P., Hinton, T., Hughes, J., Jones, C. D., Joshi, M., Liddicoat, S., Martin, G., O'Connor, F., Rae, J., Senior, C., Sitch, S., Totterdell, I., Wiltshire, A., & Woodward, S., 2011. Development and evaluation of an Earth-System model - HadGEM2. *Geoscientific Model Development*, *4*(4), 1051–1075. https://doi.org/10.5194/gmd-4-1051-2011.

Cox, P.M., Betts, R.A., Jones, C.D., Spall, S.A. and Totterdell, I.J., 2000. Acceleration of global warming due to carbon-cycle feedbacks in a coupled climate model. *Nature*, *408*(6809), pp.184-187. https://doi.org/10.1038/35041539.

Dee, D.P., Uppala, S., Simmons, A.J., Berrisford, P., Poli, P., Kobayashi, S., Andrae, U., Balmaseda, M.A., Balsamo, G., Bauer, D.P. and Bechtold, P., 2011. The ERA-Interim reanalysis: Configuration and performance of the data assimilation system. *Quarterly Journal of the royal meteorological society*, *137*(656), pp.553-597. https://doi.org/10.1002/qj.828.

Engelbrecht, F.A., McGregor, J.L. and Engelbrecht, C.J., 2009. Dynamics of the Conformal-Cubic Atmospheric Model projected climate-change signal over southern Africa. *International Journal of Climatology: A Journal of the Royal Meteorological Society*, *29*(7), pp.1013-1033. https://doi.org/10.1002/joc.

Engelbrecht, F. A., Landman, W. A., Engelbrecht, C. J., Landman, S., Bopape, M. M., Roux, B., McGregor, J. L., & Thatcher, M., 2011. Multi-scale climate modelling over Southern Africa using a variable-resolution global model. *Water SA*, *37*(5), 647–658. https://doi.org/10.4314/wsa.v37i5.2.

Entekhabi, D., Njoku, E. G., O'Neill, P. E., et al. (2010). The Soil Moisture Active Passive (SMAP) Mission. *Proceedings of the IEEE*, 98(5), 704–716. https://doi.org/0.1109/JPROC.2010.2043918

Ernst, Y., Archibald, S., Balzter, H., Chevallier, F., Ciais, P., Fischer, C. G., Gaubert, B., Higginbottom, T., Higgins, S., Lawal, S., Lacroix, F., Lauerwald, R., Lourenco, M., Martens, C., Mengistu, A. G., Merbold, L., Mitchard, E., Moyo, M., Nguyen, H., … Scholes, R. (2024). The African Regional Greenhouse Gases Budget (2010–2019). *Global Biogeochemical Cycles*, *38*(4), e2023GB008016. doi: 10.1029/2023GB008016.

Eyring, V., Cox, P.M., Flato, G.M., Gleckler, P.J., Abramowitz, G., Caldwell, P., Collins, W.D., Gier, B.K., Hall, A.D., Hoffman, F.M. and Hurtt, G.C., 2019. Taking climate model evaluation to the next level. *Nature Climate Change*, *9*(2), pp.102-110. https://doi.org/10.1038/s41558-018-0355-y.

Flato, G., Marotzke, J., Abiodun, B., Braconnot, P., Chou, S.C., Collins, W., Cox, P., Driouech, F., Emori, S., Eyring, V. and Forest, C., 2014. Evaluation of climate models. In *Climate change 2013: the physical science basis. Contribution of Working Group I to the Fifth Assessment Report of the Intergovernmental Panel on Climate Change* (pp. 741-866). Cambridge University Press.

Friedlingstein, P., Bopp, L., Ciais, P., Dufresne, J.L., Fairhead, L., LeTreut, H., Monfray, P. and Orr, J., 2001. Positive feedback between future climate change and the carbon cycle. *Geophysical Research Letters*, *28*(8), pp.1543-1546. https://doi.org/10.1029/2000GL012015.

Friedlingstein, P., O'Sullivan, M., Jones, M. W., Andrew, R. M., Hauck, J., Landschützer, P., Le Quéré, C., Li, H., Luijkx, I. T., Olsen, A., Peters, G. P., Peters, W., Pongratz, J., Schwingshackl, C., Sitch, S., Canadell, J. G., Ciais, P., Jackson, R. B., Alin, S. R., Arneth, A., Arora, V., Bates, N. R., Becker, M., Bellouin, N., Berghoff, C. F., Bittig, H. C., Bopp, L., Cadule, P., Campbell, K., Chamberlain, M. A., Chandra, N., Chevallier, F., Chini, L. P., Colligan, T., Decayeux, J., Djeutchouang, L. M., Dou, X., Duran Rojas, C., Enyo, K., Evans, W., Fay, A. R., Feely, R. A., Ford, D. J., Foster, A., Gasser, T., Gehlen, M., Gkritzalis, T., Grassi, G., Gregor, L., Gruber, N., Gürses, Ö., Harris, I., Hefner, M., Heinke, J., Hurtt, G. C., Iida, Y., Ilyina, T., Jacobson, A. R., Jain, A. K., Jarníková, T., Jersild, A., Jiang, F., Jin, Z., Kato, E., Keeling, R. F., Klein Goldewijk, K., Knauer, J., Korsbakken, J. I., Lan, X., Lauvset, S. K., Lefèvre, N., Liu, Z., Liu, J., Ma, L., Maksyutov, S., Marland, G., Mayot, N., McGuire, P. C., Metzl, N., Monacci, N. M., Morgan, E. J., Nakaoka, S.-I., Neill, C., Niwa, Y., Nützel, T., Olivier, L., Ono, T., Palmer, P. I., Pierrot, D., Qin, Z., Resplandy, L., Roobaert, A., Rosan, T. M., Rödenbeck, C., Schwinger, J., Smallman, T. L., Smith, S. M., Sospedra-Alfonso, R., Steinhoff, T., Sun, Q., Sutton, A. J., Séférian, R., Takao, S., Tatebe, H., Tian, H., Tilbrook, B., Torres, O., Tourigny, E., Tsujino, H., Tubiello, F., van der Werf, G., Wanninkhof, R., Wang, X., Yang, D., Yang, X., Yu, Z., Yuan, W., Yue, X., Zaehle, S., Zeng, N., and Zeng, J.: Global Carbon Budget 2024, Earth Syst. Sci. Data, 17, 965–1039, https://doi.org/10.5194/essd-17-965-2025, 2025.

Foken, T. and Wichura, B., 1996. Tools for quality assessment of surface-based flux measurements. *Agricultural and forest meteorology*, *78*(1-2), pp.83-105. https://doi.org/10.1016/0168-1923(95)02248-1.

Foken, T., Leuning, R., Oncley, S.R., Mauder, M. and Aubinet, M., 2012. Corrections and data quality control. *Eddy covariance: a practical guide to measurement and data analysis*, pp.85-131. https://doi.org/10.1007/978-94-007-2351-1_4.

GFDL, 2025. "Climate Modeling, Geophysical Fluid Dynamics Laboratory". Available at: https://www.gfdl.noaa.gov/climate-modeling/#What%20is%20a%20Global%20Climate%20Model.

Hao, Y., Mao, J., Bachmann, C.M. *et al.* Soil moisture controls over carbon sequestration and greenhouse gas emissions: a review. *npj Clim Atmos Sci* **8**, 16 (2025). https://doi.org/10.1038/s41612-024-00888-8

K.A. Heckman, A.R. Possinger, B.D. Badgley, M.M. Bowman, A.C. Gallo, J.A. Hatten, L.E. Nave, M.D. SanClements, C.W. Swanston, T.L. Weiglein, W.R. Wieder, & B.D. Strahm, Moisture-driven divergence in mineral-associated soil carbon persistence, Proc. Natl. Acad. Sci. U.S.A. 120 (7) e2210044120, https://doi.org/10.1073/pnas.2210044120 (2023).

Hazeleger, W., Severijns, C., Semmler, T., Ştefănescu, S., Yang, S., Wang, X., Wyser, K., Dutra, E., Baldasano, J. M., Bintanja, R., Bougeault, P., Caballero, R., Ekman, A. M. L., Christensen, J. H., Van Den Hurk, B., Jimenez, P., Jones, C., Kållberg, P., Koenigk, T., … Willén, U., 2010. EC-Earth: A seamless Earth-system prediction approach in action. *Bulletin of the American Meteorological Society*, *91*(10), 1357–1363. https://doi.org/10.1175/2010BAMS2877.1.

Hersbach, H., Bell, B., Berrisford, P., Hirahara, S., Horányi, A., Muñoz-Sabater, J., Nicolas, J., Peubey, C., Radu, R., Schepers, D. and Simmons, A., 2020. The ERA5 global reanalysis. *Quarterly journal of the royal meteorological society*, *146*(730), pp.1999-2049. https://doi.org/10.1002/qj.3803.

Jackson, T. J., Bindlish, R., Cosh, M. H., et al. (2012). Validation of Soil Moisture and Ocean Salinity (SMOS) soil moisture over watershed networks in the U.S. *IEEE Transactions on Geoscience and Remote Sensing*, 50(5), 1530–1543. https://doi.org/10.1109/TGRS.2011.2168533

Kawamiya, M., Hajima, T., Tachiiri, K., Watanabe, S. and Yokohata, T., 2020. Two decades of Earth system modeling with an emphasis on Model for Interdisciplinary Research on Climate (MIROC). *Progress in Earth and Planetary Science*, *7*(1), pp.1-13. https://doi.org/10.1186/s40645-020-00369-5.

Kutsch, W.L., Kolle, O., Rebmann, C., Knohl, A., Ziegler, W. and Schulze, E.D., 2008. Advection and resulting CO2 exchange uncertainty in a tall forest in central Germany. *Ecological Applications*, *18*(6), pp.1391-1405. https://doi.org/10.1890/06-1301.1.

Lee, J., Gleckler, P.J., Ahn, M.S., Ordonez, A., Ullrich, P.A., Sperber, K.R., Taylor, K.E., Planton, Y.Y., Guilyardi, E., Durack, P. and Bonfils, C., 2024. Systematic and objective evaluation of Earth system models: PCMDI Metrics Package (PMP) version 3. *Geoscientific Model Development*, *17*(9), pp.3919-3948.

Met Office, 2025. ”Unified Model”. Available at: https://www.metoffice.gov.uk/research/approach/modelling-systems/unified-model.

NCAR, 2025. ”Models: Community Earth System Model”. Available at: https://www.cesm.ucar.edu/models.

nextGEMS, 2025. ”The Earth system models used in nextGEMS, explained”. Available at: https://nextgems-h2020.eu/the-earth-system-models-used-in-nextgems-explained/.

Räsänen, M., Aurela, M., Vakkari, V., Beukes, J.P., Tuovinen, J.P., Van Zyl, P.G., Josipovic, M., Venter, A.D., Jaars, K., Siebert, S.J. and Laurila, T., 2017. Carbon balance of a grazed savanna grassland ecosystem in South Africa. *Biogeosciences*, *14*(5), pp.1039-1054. https://doi.org/10.5194/bg-14-1039-2017.

Reichle, R. H., Draper, C., Liu, Q., et al. (2017). “Assessment of the SMAP Level-4 surface and root-zone soil moisture product using in situ measurements.” *Journal of Hydrometeorology,* 18(10), 2621–2645. https://doi.org/10.1175/JHM-D-17-0063.1

Rybchak, O., du Toit, J., Delorme, J.P., Jüdt, J.K., Mukwashi, K., Thau, C., Feig, G., Bieri, M. and Brümmer, C., 2020. Multi-year CO 2 budgets in South African semi-arid Karoo ecosystems under different grazing intensities. *Biogeosciences Discussions*, *2020*, pp.1-37. https://doi.org/10.5194/bg-2020-420.

Schmid, H.P. and Lloyd, C.R., 1999. Spatial representativeness and the location bias of flux footprints over inhomogeneous areas. *Agricultural and Forest Meteorology*, 93(3), pp.195-209. https://doi.org/10.1016/S0168-1923(98)00119-1.

Steinkopf, J. and Engelbrecht, F., 2022. Verification of ERA5 and ERA-Interim precipitation over Africa at intra-annual and interannual timescales. *Atmospheric Research*, *280*, p.106427. https://doi.org/10.1016/j.atmosres.2022.106427.